The Spherical Accretion Shock Instability in the Linear Regime

John M. Blondin

Department of Physics, North Carolina State University, Raleigh, NC 27695-8202

John_Blondin@ncsu.edu

and

Anthony Mezzacappa

Physics Division, Oak Ridge National Laboratory, Oak Ridge, TN 37831-6354

mezzacappaa@ornl.gov

ABSTRACT

We use time-dependent, axisymmetric, hydrodynamic simulations to study the linear stability of the stalled, spherical accretion shock that arises in the post-bounce phase of core-collapse supernovae. We show that this accretion shock is stable to radial modes, with decay rates and oscillation frequencies in close agreement with the linear stability analysis of Houck and Chevalier. For non-spherical perturbations we find that the $l = 1$ mode is always unstable for parameters appropriate to core-collapse supernovae. We also find that the $l = 2$ mode is unstable, but typically has a growth rate smaller than that for $l = 1$. Furthermore, the $l = 1$ mode is the only mode found to transition into a nonlinear stage in our simulations. This result provides a possible explanation for the dominance of an $l = 1$ 'sloshing' mode seen in many two-dimensional simulations of core-collapse supernovae.

Subject headings: accretion—hydrodynamics—shock waves —supernovae:general—turbulence

1. Introduction

The modern paradigm for core-collapse supernovae includes a critical phase between stellar core bounce and explosion that is characterized by a stalled accretion shock, during which time neutrino heating is believed to reenergize, or at least play a critical role in

reenergizing, the stalled shock [(Burrows et al. 1995; Mezzacappa et al. 1998; Rampp & Janka 2000; Liebendoerfer et al. 2001; Buras et al. 2003; Fryer & Warren 2004)]. (For a review, see Mezzacappa (2005).) This phase is expected to last of order a few hundred milliseconds.

The past decade has seen significant interest in the multidimensional dynamics of this post-bounce accretion phase. Most two-dimensional supernova simulations exhibit strong turbulent motions below the stalled accretion shock [(Herant et al. 1992; Miller et al. 1993; Herant et al. 1994; Burrows et al. 1995; Mezzacappa et al. 1998; Buras et al. 2003; Fryer & Warren 2004)]. In the past, this turbulent flow was attributed to convection driven by the intense neutrino flux emerging from the proto-neutron star at the center of the explosion.

However, Blondin et al. (2003, hereafter Paper I) showed that the stalled accretion shock *itself* may be dynamically unstable. By using steady-state accretion shock models constructed to reflect the conditions in the post-bounce stellar core during the neutrino heating phase (as was shown in Paper I) but characterized by flat or positive entropy gradients, and as such convectively stable, Blondin et al. (2003) were able to isolate the dynamical behavior of the post-bounce accretion shock *per se*. They found that small nonspherical perturbations to the spherical accretion shock lead to rapid growth of turbulence behind the shock, as well as to rapid growth in the asymmetry of the initially spherical shock. This spherical accretion shock instability, or "SASI," is dominated by low-order modes, and is independent of any convective instability.

Clearly, once the shock wave is distorted from spherical symmetry, the non-radial flow beneath it is no longer defined solely by neutrino-driven convection. The fluid flow beneath the shock is, at least initially, a complex superposition of flows generated by convection and by the SASI-distorted shock. Once the shock wave is distorted, it will deflect radially infalling material passing through it, leading to highly nonradial flow beneath it. With time, the fluid flow beneath the shock may in fact be determined by the SASI and not by convection. Instabilities such as neutrino-driven convection may be important only at early times in aiding the neutrino heating (Herant et al. 1994; Burrows et al. 1995; Mezzacappa et al. 1998; Buras et al. 2003; Fryer & Warren 2004) and in setting the shock standoff radius while the explosion is initiated. The standoff radius will in turn determine the time scale over which the SASI may develop.

Janka (2001) provides a qualitative description of this post-bounce accretion phase in terms of a simple hydrodynamic model, with the intent of providing an analytic model that can be used to investigate the conditions necessary for a successful supernova shock. In this picture the post-bounce phase is described by a standing accretion shock with outer core material raining down on the shock at roughly half the free-fall velocity. After traversing the

turn requires a large number of computational zones and a very small time step due to the Courant condition: $\Delta t < \Delta r/c_s$. As an extreme example, to simulate a model with $r_* = 0.01$ required 200,000,000 timesteps.

These simulations do two important things: they confirm the linear stability analysis of HC, and they validate our time-dependent numerical model.

5. Linear Evolution of the SASI

We performed a series of two-dimensional axisymmetric simulations following the same procedure outlined above for one dimension, down to the same radial gridding for a given model. We experimented with a variety of ways to perturb the equilibrium solution with the goal of exciting a single mode (in terms of spherical harmonics) with as little power in other modes as possible. This goal was best achieved when using density enhancements in the preshock gas as had been used in 1D. These density variations were typically between 0.1% and 1%; large enough to excite the instability but small enough that the perturbations could grow in amplitude by more than an order of magnitude while still remaining small. This extended regime of linear growth facilitated an accurate measurement of the linear growth rate. As in Paper I, all of the two-dimensional simulations were unstable. Here we attempt to quantify the growth rate of this instability in the linear regime as a function of the wave number.

To track the importance of various modes affecting the stability of a spherical accretion shock, the evolution was tracked using Legendre polynomials. Again, after trying several methods, we found the best approach was to first integrate the amplitude in a given harmonic for a fixed radius,

$$G(r) = \int A(r,\theta) P_l(\cos\theta) d\cos\theta \tag{7}$$

and then integrate the power for that harmonic over radius:

$$Power = 2\pi \int \left[G(r)\right]^2 r^2 dr \tag{8}$$

where $A(r,\theta)$ represents some local quantity affected by the perturbed flow, e.g., entropy or pressure, and P_l is the Legendre polynomial of order l.

An example of the linear growth of the SASI is shown in Figure 3 for $r_* = 0.2$. These simulations exhibit a well-defined regime of exponential growth spanning at least an order of magnitude in amplitude. The beginning of a simulation is typically marked by a complex pattern of waves, but given an appropriate initial perturbation, a single mode soon dominates

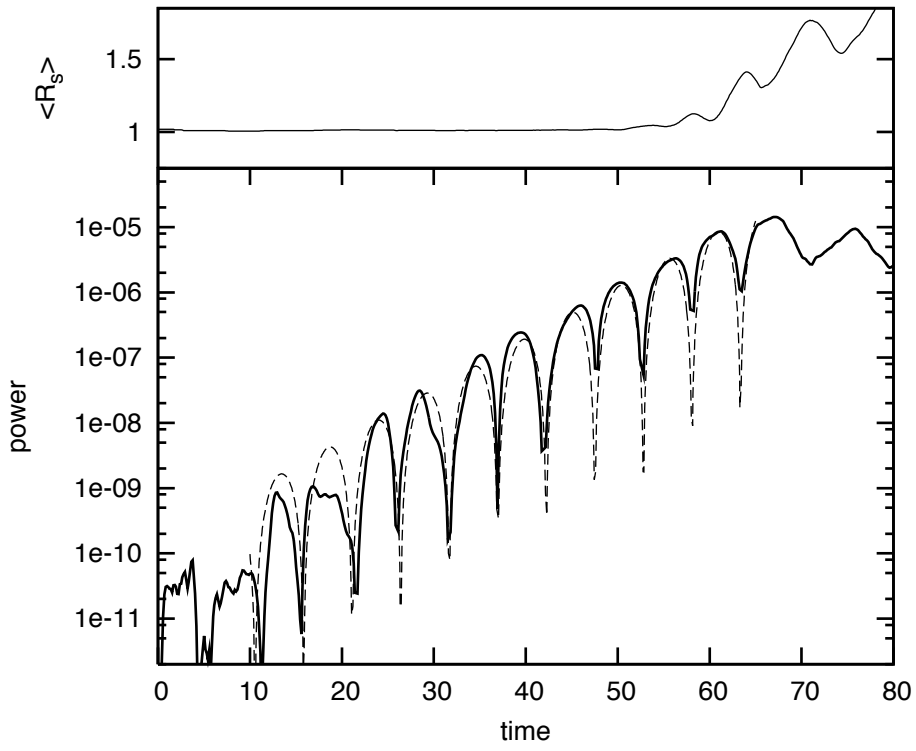

Fig. 3.— The growth of the SASI in a simulation with $r_* = 0.2$ is quantified here by the power in the perturbed entropy for the $l = 1$ mode (solid line). The best fit to this growth curve is shown as a dashed line. The SASI becomes nonlinear at a time around $t \approx 60$, as shown by the deviation of $\langle R_s \rangle$ from unity.

the evolution. To provide guidance on the relevance of the linear regime, we also show the angle-averaged shock radius throughout the evolution. During the linear regime, when perturbations to the spherical accretion flow are small, we expect the shock to remain nearly stationary. Once the average shock radius begins to deviate substantially from unity, the SASI has entered the non-linear regime.

As in the analysis of the one-dimensional simulations, we can fit these growth curves from two-dimensional simulations with an exponentially growing sinusoid. In this case, we are fitting the power, not the radius:

$$F(t) = F_1 e^{2\omega_r t} \sin^2(\omega_i t + \delta). \tag{9}$$

The fitted frequencies are shown in Figure 4 for four different values of r_* (0.5, 0.3, 0.2, and 0.1). We did not attempt simulations for smaller values because they would have required an extremely long integration, and the results for the $r_* = 0.1$ model were sufficiently noisy that we did not expect to be able to extract clean growth rates from more extended models. Note, however, that the growth rate of the $l = 1$ mode appears to be decreasing for very extended shocks and that the $l = 0$ mode becomes unstable for $r_* < .05$.

We do not consider values of r_* larger than 0.5 because this would not be consistent with our fundamental starting assumption of having conditions near explosion and a postshock gas described by a single adiabatic index. Under such conditions, we would have a large heating region dominated by radiation and a thin cooling layer at its base. A larger value of r_* would imply a larger cooling region and, generally, a postshock region composed of gases with different adiabatic indices.

We could not isolate modes with values of $l > 2$, nor could we adequately measure the growth of the $l = 2$ mode in the most extended models with $r_* = 0.1$. The results for the spherically symmetric mode ($l = 0$) are taken from the one-dimensional simulations. As expected, the frequency of oscillation is a monotonically increasing function of the wavenumber. The growth rate, however, is not. In all cases we found that $l = 1$ is the most unstable, and is always unstable.

At late times the evolution is always dominated by the $l = 1$ mode. In fact, this is the only mode that we have observed to reach a nonlinear stage. We show in Figure 5 the growth of the different modes in a simulation for which we carefully excited the $l = 2$ mode and not the $l = 1$ mode. While the $l = 2$ mode grows substantially over the course of a dozen oscillations, it stops growing before reaching the nonlinear stage. In contrast, the $l = 1$ mode grows up out of the noise and becomes nonlinear at a time of about $t \approx 120$. We speculate that the linear growth of the $l = 2$ mode stalls because power in that mode is lost to the rapidly growing $l = 1$ mode. Note that the power in $l = 1$ is very chaotic during this episode

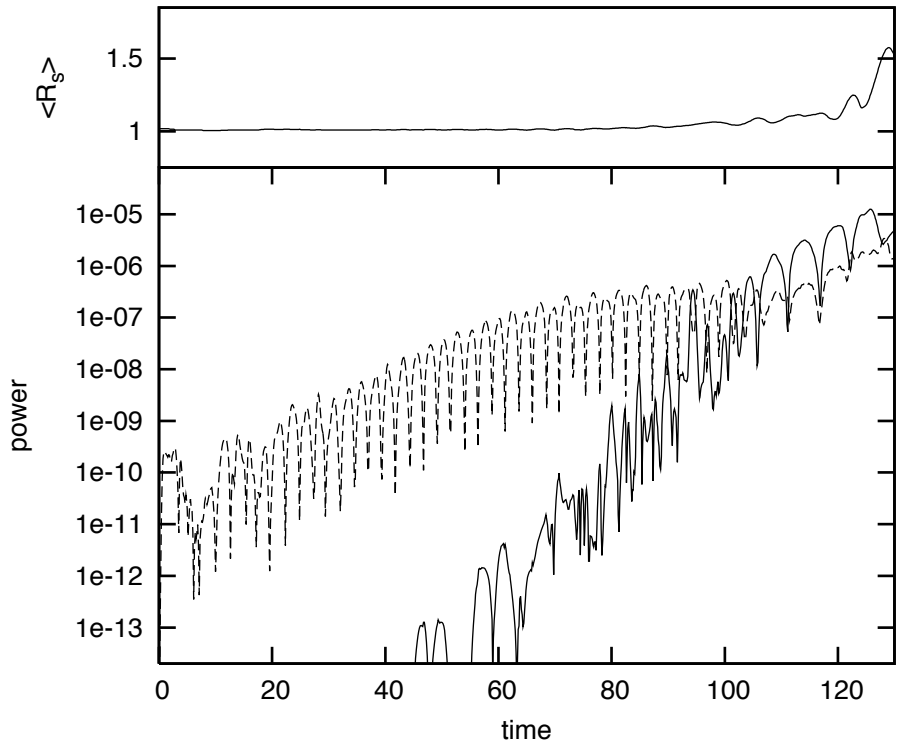

Fig. 5.— The growth of the SASI in a simulation excited with the $l = 2$ mode (dashed line) but dominated at late times by the $l = 1$ mode (solid line). The SASI becomes nonlinear at a time around $t \approx 120$, once the $l = 1$ mode becomes dominant.

Figure 7, the outward shock displacement leads to a smaller pressure immediately behind the shock. However, given that the postshock pressure increases with decreasing radius as r^{-4}, the postshock pressure for the perturbed shock will be greater than the postshock pressure for the unperturbed shock at each radius below the radius of the original unperturbed shock. This is illustrated with the two cases shown in Figure 7. The postshock pressure immediately behind the shock for the perturbed shock at radius 1.1 is lower than the postshock pressure immediately behind the unperturbed shock at radius 1.0 given the decrease in the preshock ram pressure given by the dashed line. However, at each radius below 1.0 the postshock pressure for the perturbed shock is higher than the postshock pressure for the unperturbed shock.

There is an additional effect on the immediate post-shock pressure due to the change in shock velocity. As the shock is being pushed outward, the local shock velocity is larger than for a stationary shock at that radius, leading to a slightly higher post-shock pressure. Note that the change in pressure due to shock velocity is out of phase with respect to the change in pressure due to shock displacement, with the former peaking as the shock is moving outward, and the latter peaking at a phase $\pi/2$ later when the shock has reached its maximum extent. Nonetheless, both effects act to amplify the pressure variation of the standing wave. For the observed frequencies of the $l = 1$ mode of the SASI, the effect of changing shock velocity is a few times smaller than the change in ram pressure due to shock displacement.

The linear phase of the SASI is characterized by a nearly spherical accretion shock and approximately radial post-shock flow. Once the amplitude of the standing pressure wave becomes large enough to significantly break the spherical symmetry of the accretion shock, the SASI enters the non-linear phase. In this phase the radially infalling gas above the shock strikes the shock surface at an oblique angle, generating strong, non-radial post-shock flow. This transition from the linear to non-linear phase is illustrated in Figure 8. The effect of a distorted shock on the post-shock flow is quite dramatic even for the relatively slight changes in shock position shown in the second frame of Figure 8. Although the accretion shock is nearly spherical in this frame, it is significantly displaced upward. As a result, the post-shock flow is no longer radial, and in some regions is almost entirely tangential to the radial direction. As a consequence of this non-radial flow, perturbations generated on one side of the shock can be advected across the interior and over to the other side of the accretion cavity. For example, the second frame in Figure 8 shows a shell of high-entropy gas (shown in blue) in the upper hemisphere being advected around the central star and toward the lower hemisphere.

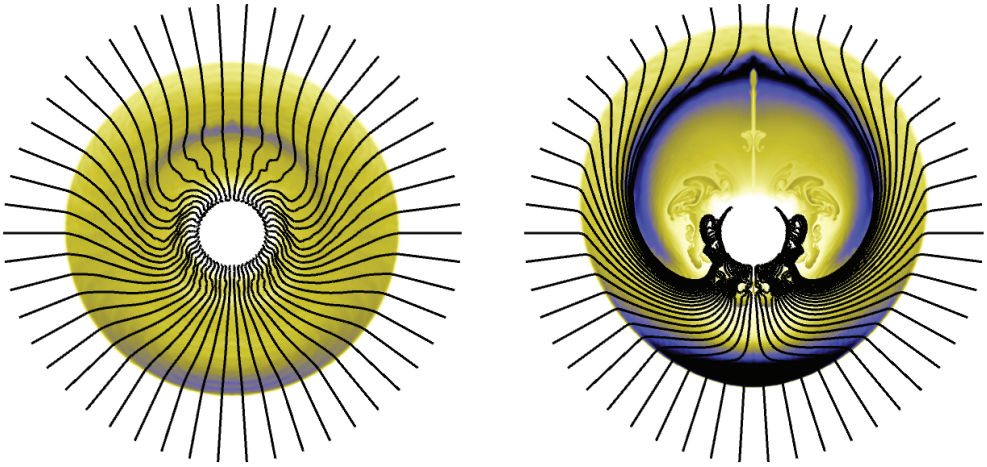

Fig. 8.— The transition from the linear to the non-linear regime is illustrated with these two images spanning one oscillation period. The color shows positive (blue) and negative (yellow/white) deviations to the equilibrium value of gas entropy, and the lines represent streamlines integrated along the instantaneous velocity field. The transition to the nonlinear regime is largely characterized by the transition from radial to nonradial flow. An mpeg animation of this transition is available on line.